Detached-Eddy Simulations of Full Aircraft Experiencing Massively Separated Flows

S.A. Morton [1], J.R. Forsythe [2], K.D. Squires[3], R.M. Cummings[4]

1. *Scott.Morton@usafa.af.mil, United States Air Force Academy, Department of Aeronautics, USAF Academy, CO 80840-6400, USA*
2. *Forsythe@cobaltcfd.com, Cobalt Solutions, LLC., 270 Cape Romain Dr., Colorado Springs, CO 80920, USA*
3. *squires@asu.edu, MAE Dept, Arizona State University, Tempe, AZ, 85287, USA*
4. *Russ.Cummings@usafa.af.mil, United States Air Force Academy, Department of Aeronautics, USAF Academy, CO 80840-6400, USA*

Corresponding author ***S.A. Morton***

Abstract

A high resolution turbulence treatment for massively separated flows is presented for fighters at flight Reynolds numbers. The method is Detached Eddy Simulation (DES), a hybrid Reynolds averaged Navier-Stokes – Large Eddy Simulation technique that can accurately capture attached boundary layers at flight Reynolds numbers, while still reproducing the unsteady loads associated with massively separated flow. Three examples of US Department of Defense aircraft, the F-15E, F/A-18C, and F/A-18E, are used as test cases to show the utility of Detached Eddy Simulation in capturing nonlinear phenomena such as wing buffet, vortex breakdown, and abrupt wing stall. Comparison with either flight test or experiment is also accomplished for these cases.

Keyword: Detached Eddy Simulation, Massively Separated Flows, Post-stall Aerodynamics, Vortex Breakdown, Abrupt Wing Stall

1. *Introduction*

Design of flight vehicles currently relies on three methods of analysis: wind tunnel testing, flight testing, and computational simulation. It is well known that wind tunnel testing for aeroelasticity or flight mechanics is extremely expensive due to the need to not only represent the aerodynamics properly through scaling parameters such as the Reynolds number and Mach number, but also the scaling for dynamic motion. In addition, wind tunnel testing an aeroelastic model is more likely to produce a catastrophic failure of the model than in aerodynamic testing. It is this combination that significantly increases the cost of wind tunnel testing and, consequently, the availability of tunnels capable of performing aeroelastic testing is quite restrictive. Even if the cost of wind tunnel testing is accepted, there are very few facilities capable of testing at flight Reynolds numbers.

Flight testing for aeroelasticity or flight motion is typically incapable of impacting the design cycle in a positive way because of the investment in tooling and analysis necessary to create a flight vehicle. In general, flight testing is used to verify predictions or resolve problems discovered during previous tests. Flight tests are the most expensive form of analysis due to the man-hours, manufacturing costs, and equipment costs associated with such a test.

It is the third form of analysis, computational simulation, that appears to be well suited to positively affect the design cycle of future aircraft. Although much of an aircraft's flight envelope can be analyzed adequately by current methods, certain regimes such as low speed, high angle of attack, and transonic flight require aerodynamic models sophisticated enough to accurately predict separation caused by shock interactions or high angles of attack and other nonlinear phenomenon such as vortex breakdown. It is in these regions that current methods are least likely to perform adequately and in which Air Force aircraft operate the majority of the time.

In general, knowledge of the aeroelastic properties of military aircraft is useful for understanding aspects such as limit-cycle oscillation, flutter, and elastically driven flow separation. An improved characterization of these and other effects gained in military applications can lead to

improvements in general aviation, and possibly the development of "dual use" technologies. A simulation tool is clearly useful since it is difficult to determine aeroelastic properties of the disparate configurations comprising Air Force aircraft by extrapolating available data.

While advances have taken place in areas such as grid generation and fast algorithms for solutions of systems of equations, CFD has remained limited as a reliable tool for prediction of inherently unsteady flows at flight Reynolds numbers. Current engineering approaches for prediction of unsteady flows are based on solution of the Reynolds-averaged Navier-Stokes (RANS) equations. The turbulence models employed in RANS methods necessarily model the entire spectrum of turbulent motions. While often adequate in steady flows with no regions of reversed flow, or possibly exhibiting shallow separation, it appears inevitable that RANS turbulence models are unable to accurately predict flows characterized by massive separation. Unsteady, massively separated flows are characterized by geometry-dependent and three dimensional turbulent eddies. These eddies, arguably, are what defeat RANS turbulence models, of any complexity.

To overcome the deficiencies of RANS models for predicting massively separated flows, Spalart et.al.[1] proposed Detached-Eddy Simulation (DES) with the objective of developing a numerically feasible and accurate approach combining the most favorable elements of RANS models and Large Eddy Simulation (LES). The primary advantage of DES is that it can be applied at high Reynolds numbers as can Reynolds-averaged techniques, but also resolves geometry-dependent, unsteady three-dimensional turbulent motions as in LES. The unstructured finite-volume solver *Cobalt* [2] has been used in conjunction with DES successfully on a number of complex problems, including a supersonic base flow [3], delta wing vortex breakdown [4], a square with rounded corners [5], the F-15E at high angle of attack [5], the F/A-18C with tail buffet [6], and the F/A-18E with unsteady shock buffet [7].

The specific aim of this work is to demonstrate detached-eddy simulations of three configurations that highlight the ability of the method to capture three distinct flowfield types: post-stall separation, vortex breakdown induced tail buffet, and abrupt wing stall. These three flowfield types will be demonstrated on three full aircraft configurations currently in the US Department of Defense inventory (F-15E, F/A-18C, and F/A-18E) at operational flight conditions.

2. Numerical Method

In this section a brief description of the numerical method is provided. Full details of the computational scheme are presented in Ref. [2]. Solutions for all configurations were computed with the commercial version of Cobalt developed by Cobalt Solutions, LLC. Cobalt solves the unsteady, three-dimensional, compressible Navier-Stokes equations on a hybrid unstructured grid. The code has several choices of turbulence models, including Spalart Almaras (SA), and Menter's Shear Stress Transport (SST) RANS, as well as DES versions of SA and SST. All simulations were computed on unstructured meshes with prisms in the boundary layer and tetrahedra elsewhere. The computational meshes were generated with the software packages GridTool [8] and VGRIDns [9].

2.1 Turbulence Models

For simulation of turbulent flows, the governing equations are suitably averaged, yielding turbulent stresses that require a model. A Boussinesq approximation is invoked in the momentum equations and the turbulent eddy viscosity (m_t) is used to relate the stresses to the strain rate. The turbulent heat flux is also modeled using a gradient-transport hypothesis, requiring specification of a turbulent thermal conductivity, k_t. The Reynolds analogy is applied and the turbulent heat flux is modeled using a constant turbulent Prandtl number of 0.9. Using turbulent eddy viscosity and turbulent conductivity, the variable m is replaced by $(m + m_t)$ and k is replaced by $(k + k_t)$ in the governing equations.

2.1.1 Spalart-Allmaras

The Spalart-Allmaras [10] one equation model (SA) solves a single partial differential equation for a working variable $\tilde{n}$ which is related to the turbulent viscosity. The differential equation is

derived by "using empiricism and arguments of dimensional analysis, Galilean invariance and selected dependence on the molecular viscosity" [10]. The model includes a wall destruction term that reduces the turbulent viscosity in the laminar sub layer. The model takes the form,

$$\frac{D\tilde{n}}{Dt} = c_{b1}\tilde{S}\tilde{n} - c_{w1} f_w \left[\frac{\tilde{n}}{d}\right]^2 + \frac{1}{s}\left[\nabla\cdot\left((n+\tilde{n})\nabla\tilde{n}\right) + c_{b2}(\nabla\tilde{n})^2\right].$$

The turbulent kinematic viscosity is obtained from,

$$n_t = \frac{m_t}{r} = \tilde{n} f_{v1}, \qquad f_{v1} = \frac{c^3}{c^3 + c_{v1}^3}, \qquad c \equiv \frac{\tilde{n}}{n}$$

where S is the magnitude of the vorticity given by

$$S = |w| = \left|\nabla\times\left(u\hat{i} + v\hat{j} + w\hat{k}\right)\right|,$$

and the modified vorticity is,

$$\tilde{S} \equiv S + \frac{\tilde{n}}{k^2 d^2} f_{v2}, \qquad f_{v2} = 1 - \frac{c}{1 + c f_{v1}},$$

where d is the distance to the closest wall. The wall destruction function f_w is,

$$f_w = g\left[\frac{1+c_{w3}^6}{g^6 + c_{w3}^6}\right]^{\frac{1}{6}},$$

and

$$g = r + c_{w2}\left(r^6 - r\right), \qquad r \equiv \frac{\tilde{n}}{\tilde{S}k^2 d^2}.$$

The turbulent viscosity is obtained from the turbulent kinematic viscosity by $m_t = r n_t$.

The model coefficients are,

$c_{b1} = 0.1355$ $\quad s = 2/3$ $\quad c_{b2} = 0.622$

. $k = 0.41$ $\quad c_{w1} = c_{b1}/k^2 + (1+c_{b2})/s$ $\quad c_{w2} = 0.3$

$c_{w3} = 2$ $\quad c_{v1} = 7.1$

2.1.2 Detached-Eddy Simulation

The Detached-Eddy Simulation method was proposed by Spalart et al. [1] and was originally based on the Spalart-Allmaras one equation RANS turbulence model (detailed above) with a more detailed presentation in Ref. [11]. The wall destruction term presented above is proportional to $(\tilde{n}/d)^2$, where d is the distance to the wall. When this term is balanced with the production term, the eddy viscosity becomes proportional to $\hat{S}d^2$ where $\hat{S}$ is the local strain rate. The Smagorinski LES model varies its sub-grid scale (SGS) turbulent viscosity with the local strain rate, and the grid spacing: $n_{SGS} \propto \hat{S}\Delta^2$, where $\Delta = \max(\Delta x, \Delta y, \Delta z)$. If d is replaced with Δ in the wall destruction term, the SA model will act as a Smagorinski LES model.

To exhibit both RANS and LES behavior, d in the SA model is replaced by

$$\tilde{d} = \min(d, C_{DES}\Delta).$$

When $d << \Delta$, the model acts in a RANS mode and when $d >> \Delta$ the model acts in a Smagorinski LES mode. Therefore the model switches into LES mode when the grid is locally refined.

DES was implemented in an unstructured grid method by Forsythe et. al. [3]. They determined the C_{DES} constant should be 0.65, consistent with the structured grid implementation of Spalart et. al. [11] when the grid spacing Δ was taken to be the longest distance between the cell center and all of the neighboring cell centers.

A Newton sub-iteration method is used in the solution of the system of equations to improve time accuracy of the point implicit method and approximate Jacobians. In the calculations presented below, a typical number of three Newton sub-iterations is used for all time-accurate cases.

2.2 Grid Generation

Spalart (Ref. 21) described the process of grid design and assessment for DES, defining important regions of the solution and offering guidelines for grid densities within each region. The "Young-Person's Guide" [12] (YPG) forms a basis for interpretation of many of the results presented below. One of the traditional motivations for using unstructured grids has been the ability to rapidly create grids around complex geometries. There are other positive attributes of unstructured grids that are relevant to DES. Most notably, it is possible to concentrate points in the region of interest (i.e. the vortex core or aft of breakdown) and rapidly coarsen the grid away from these areas. This region of interest was termed the "focus region" in the YPG. Another advantage exploited in the present study is the isotropic cells generated in the LES region by most unstructured grid generation packages. The YPG reference describes the desirability of having nearly isotropic grid cells in the focus region in which unsteady, time-dependent, features are resolved. For this reason, unstructured grids are good candidates for use in DES because near isotropy of the grid cells in the LES region is assured by most grid generation packages.

In Ref. [13] the YPG guidelines were applied to three massively separated flows of interest: forebody in a cross-flow, flow over a delta wing at 27^o angle of attack, and the flow over an F-15E at 65^o angle of attack (the subject of this work). In the latter two cases an extensive grid sensitivity study was performed by systematically varying the grid by a scale parameter allowing a very consistent analysis of grid effects when using the DES method of computing massively separated flows.

Another important grid technology that is particularly well suited for DES is adaptive mesh refinement. Pirzadeh [14] presented a method based on a tetrahedral unstructured grid technology developed at NASA Langley Research Center with application to two configurations with vortex dominated flowfields. The large improvement of the adapted solutions in capturing vortex flow structures over the conventional un-adapted results was demonstrated by comparisons with wind tunnel data. Pirzadeh showed the numerical prediction of these vortical flows was highly sensitive to the local grid resolution and he also stated that grid adaptation is essential to the application of CFD to these complicated flowfields. His most successful computations were performed using an inviscid method due to the inadequacies of standard turbulence models in computing these complicated flowfields. For the current work a mean flow solution on a baseline grid is used to create an adaptively refined mesh and the new grid is used with DES to compute the unsteady flowfield.

2.3 Summary of the Method

The method for simulating full aircraft at flight Reynolds numbers is as follows:

1. Use a time accurate unstructured grid solver to allow rapid turn around of grids on complex configurations- must have at least second-order spatial and temporal accuracy.
2. Use DES as the underlying turbulence treatment to obtain accurate unsteady loads and mean quantities – this requires a low dissipation solver.
3. Use Adaptive Mesh Refinement to improve grid resolution in critical areas with nonlinear flowfield phenomena.

3. Results

This section presents results for three aircraft, the F-15E, F/A-18C, and F/A-18E, operating at flight conditions consistent with massively separated flows. The first two cases demonstrate the ability of DES to accurately predict post-stall aerodynamics, whereas the third case demonstrates prediction of separated flow due to shock-vortex-boundary layer interactions at transonic speeds.

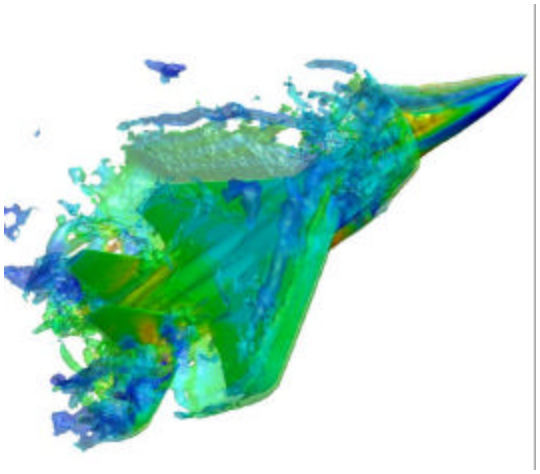

Figure 1: F-15E instantaneous iso-surface of vorticity alpha=65^o and Re=13.6 X 10^6.

3.1 F-15E

Detached-Eddy Simulation (DES) was used to predict the massively separated flow around an F-15E at 65^o angle-of-attack (see Fig. 1). The calculations were performed at flight test conditions corresponding to a chord-based Reynolds number of 13.6 X 10^6 and a Mach number of 0.3. The calculations were performed using unstructured grids in which the baseline mesh was comprised of 5.9 X 10^6 cells with prisms in the boundary layer and isotropic tetrahedra in other regions.

		C_L	C_D	C_M	$\%C_L$	$\%C_D$	$\%C_M$
	Exp	0.781	1.744	-0.466			
	Coarse	0.747	1.677	-0.431	-4.25%	3.86%	-7.62%
DES	Baseline	0.736	1.616	-0.495	-5.70%	-7.35%	6.10%
	Fine	0.759	1.648	-0.457	-2.81%	-5.52%	-2.00%
	Coarse	0.855	1.879	-0.504	9.49%	7.73%	8.17%
S-A	Baseline	0.852	1.867	-0.523	9.09%	7.05%	12.22%
	Fine	0.860	1.880	-0.507	10.22%	7.78%	8.72%

Table 1: Comparison of computed and flight test derived loads for the F-15E at alpha=65^o and Re=13.6 X 10^6.

Mesh spacings from solid surfaces to the first cell center nearest the wall were within one viscous unit. The influence of the mesh was assessed using calculations performed on two other grids: a coarser mesh of 2.85 X 10^6 cells and a finer mesh of 10 X 10^6 cells. In addition, the influence of the timestep was investigated using the baseline mesh and two simulations with timesteps a factor of two and four larger than the value used in the baseline calculations. DES predictions were assessed via comparison to flight-test data as well as solutions on the same grids of the Reynolds-averaged Navier-Stokes (RANS) equations. Both RANS and DES predictions show a convergence towards flight-test data with increases in grid density and reductions in the timestep. Time-dependent RANS predictions were obtained using the Spalart-Allmaras model and evolve to steady solutions. DES predictions of the lift, drag, and pitching moment coefficients agree to within 5% of the flight test database (see Table 1).

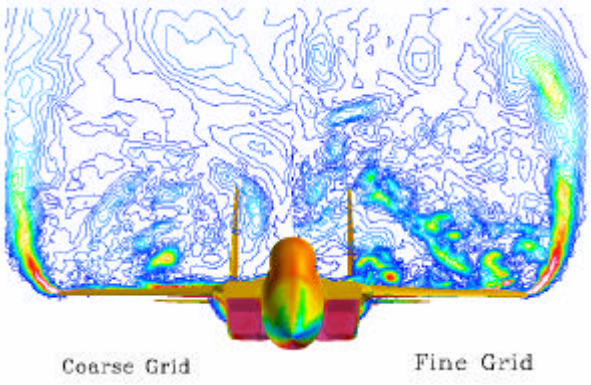

Figure 2: Instantaneous vorticity contours at 680 inches behind the aircraft reference point. Coarse grid prediction in the left-half plane (2.85 X 10^6 cells), fine grid result in the right half plane (10 X 10^6 cells).

DES predictions show that the wake region is characterized by complex and chaotic three-dimensional structures exhibiting a reasonable range of length and time scales (Fig. 1). Fig. 2 depicts a cross-plane of instantaneous vorticity for two different mesh densities. The left-half plane shows the coarse grid solution and the right-half plane shows the fine grid solution. The additional eddy content is obvious in the finer grid solution. The additional eddy content contributes to the flat pressure profile common over wings and empennage at post-stall conditions. Additional details of this flowfield can be found in Ref. [5].

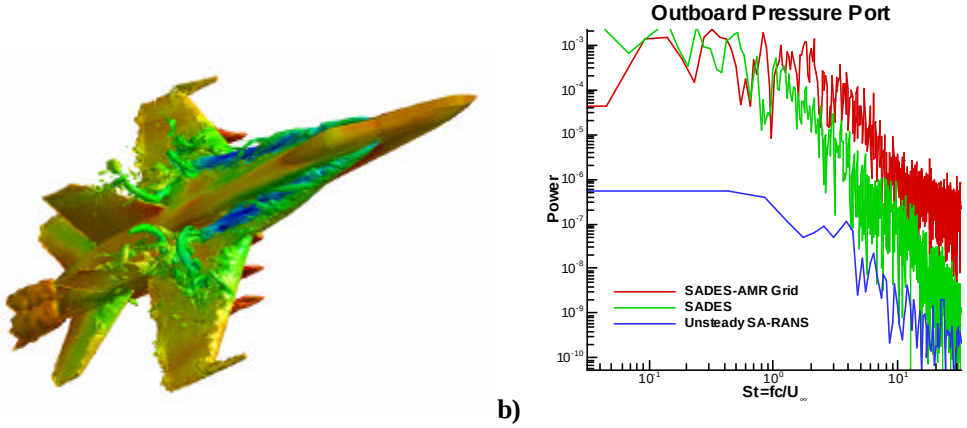

a) **b)**

Figure 3: a) Flow visualization of vortex breakdown over the F/A-18C. Iso-surface of vorticity colored by pressure. b) Power spectral density analysis of tail pressure ports for both DES and RANS.

3.2 F/A-18C

A well known issue of the pre-production F/A-18 is vortex induced tail buffet. An F/A-18*C* was simulated using DES at conditions consistent with tail buffet, an angle of attack of 30^{o}, freestream Mach number of 0.2755, and a mean aerodynamic chord based Reynolds number of 13.9 X 10^{6} [6]. 25). Fig. 3a depicts an iso-surface of vorticity colored by pressure. The leading-edge extension vortex breakdown is evident as well as the wing leading-edge vortex. The post-breakdown windings and turbulent eddies that contribute to tail buffet are also evident. Fig. 3b is a plot of a power spectral density analysis of an outboard tail pressure port. Comparison of the power for the DES baseline grid solution, DES AMR grid solution, and RANS solution demonstrates the inability of RANS methods to capture the unsteadiness contributing to tail buffet. The orders of magnitude increase in power for the DES solutions over RANS gives evidence of how unsteady motion is damped by RANS methods and captured by the DES methods. Fig. 3b also demonstrates the improvement in the resulting power when an AMR grid is used.

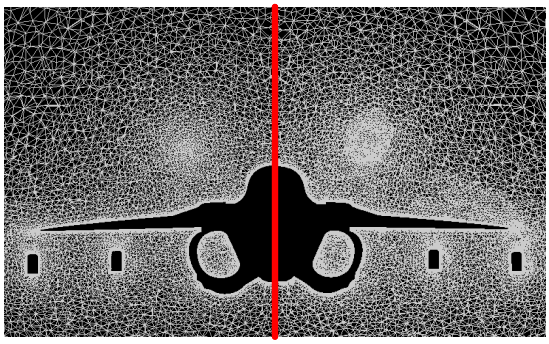

Figure 4: Baseline grid of 5.9 million cells (left) and AMR grid of 6.5 million cells (right) at a station 410 inches aft of the origin.

Fig. 4 depicts a cross-plane at a station 410 inches aft of the origin for both the baseline grid and the AMR grid. It is obvious from Fig. 4 that the AMR grid has enhanced resolution in the core of the LEX vortex, the separated region over the wing, at the wingtip pylons, and the under wing pylons. These enhanced grid regions are due to the AMR based on a vorticity iso-surface corresponding to separation regions at these locations and due to the vorticity in the LEX vortex core.

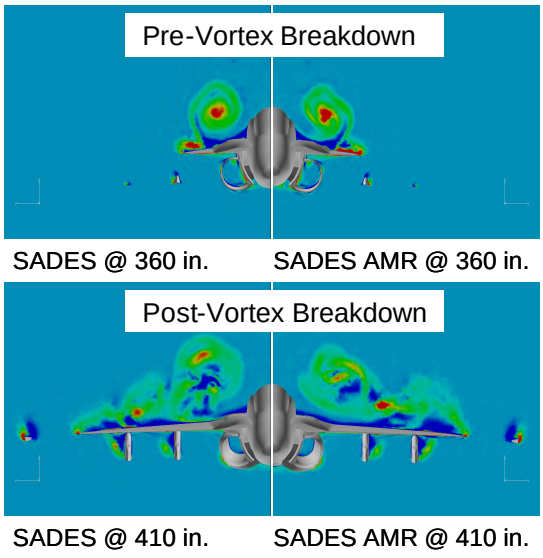

Figure 5: Cross-planes of vorticity at two stations (pre- and post-breakdown) on the F/A-18C for the baseline grid (left) and the AMR grid (right).

In Fig. 5, two cross-planes of streamwise vorticity are shown for the baseline grid solution (left) and the AMR grid solution (right) for a particular instant in time. For ease of comparison, the sense of the vortex is redefined to match the color scheme on the left wing with the right wing even though these vortices rotate in opposite directions. The pre-breakdown cross-plane at 360 inches aft of the origin shows that the AMR grid solution provides better definition of the complex vortical flowfields encountered at this angle of attack. A primary LEX vortex core is observed (red) over the top of a secondary vortex (blue), as well as a wing vortex (blue) is observed just outboard of the LEX secondary vortex. Neither this wing vortex nor the LEX vortex are as well defined on the baseline grid as the AMR grid at this pre-breakdown location. Since the flowfield aft of breakdown varies tremendously with time and these cross-planes are instantaneous, no conclusions can be made for the accuracy of the AMR grid solution versus the baseline grid solution. The ability of DES to capture vortex breakdown and the associated unsteady loads provides a method of computing tail buffet on twin tail fighter aircraft.

3.3 F/A-18E

DES predictions of the pre-production F/A-18E were reported by Forsythe and Woodson [7] as part of the Abrupt Wing Stall (AWS) research program. During envelope expansion flights of the F/A-18E/F in the Engineering and Manufacturing Development phase, the aircraft encountered uncommanded lateral activity, which was labelled "wing drop." The wing drop events were traced to an abrupt wing stall on either the left or right wing panel, causing a sudden and severe roll-off in the direction of the stalled wing. A production solution was developed that eliminated the wing drop tendency.

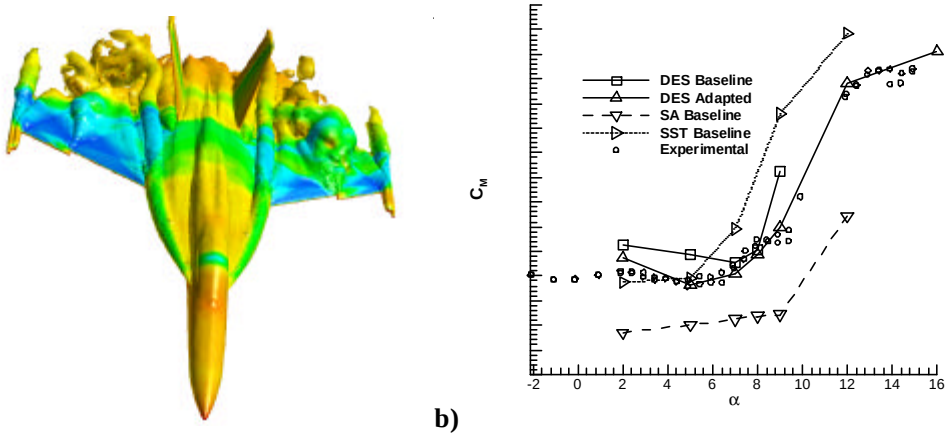

a) **b)**

Figure 4: a) Flow visualization of shock induced unsteady flow over the preproduction F/A-18E at a transonic Mach number. Iso-surface of vorticity colored by pressure. b) Pitching moment coefficient for DES, SA, SST, and experiments.

Wind tunnel measurements of the pre-production F/A-18E were made by Schuster and Byrd [15], revealing highly unsteady, low frequency shock oscillations on the wing, which were identified as a potential trigger event for the "wing drop." RANS methods were unable to reproduce these shock oscillations, even though the computations were performed in a time-accurate fashion (i.e., URANS).

Simulations of half of the F/A-18E were calculated with a solution-adapted 9 X 10^6 cell grid for 8000 time steps requiring 9000 cpu hours on a Compaq ES45 (3 days on 128 processors). Full aircraft calculations were also performed on meshes comprised of 18 X 10^6 cells requiring twice the number of cpu hours. Shown in Fig. 4a is a flow visualization of the F/A-18E DES prediction of the full span. An iso-surface of vorticity colored by pressure is shown for the flow at Mach 0.9 and 9 degrees angle-of-attack. Experimental measurements showed that the shock oscillated from the leading edge flap hinge line to about mid-chord at this angle of attack. The DES predictions also resolved this shock motion, although with slightly less travel. In the instantaneous image shown in the figure, the starboard shock has retreated from the flap hinge line whereas the port side has not,

creating an asymmetry. The separation bubble behind the port shock is relatively large, and well resolved in the DES calculation, due to the solution-adapted grid. The minimum, maximum, and average pressures along the chord compared favourably to the unsteady experimental measurements throughout the AWS angle-of-attack range as summarized by Forsythe and Woodson [7]. The pitching moment coefficient depicted in Fig. 4b shows the excellent comparison of DES with an adapted mesh and the experiments. It also demonstrates how far off the RANS simulations are for this case.

4. Conclusions and Recommendations

Detached eddy simulations of three full aircraft have been presented to show the utility of the method for fighter aircraft experiencing massively separated flow. All of the simulations were accomplished at flight Reynolds numbers and compared with flight or wind tunnel tests for validation. The F-15E demonstrated the accuracy with which DES can be used to predict massively separated flow emanating from the wing leading edge at post-stall conditions. The F/A-18C simulations demonstrated the ability of the method to accurately predict vortex breakdown, a contributor to tail buffet, over high alpha lift devices. The F/A-18C simulations also demonstrated how adaptive mesh refinement can be used to enhance grid resolution in the vortex breakdown region to capture the relevant unsteadiness. The F/A-18E simulations demonstrated the applicability of the method to the transonic nonlinear aerodynamic phenomena of abrupt wing stall, which is created by a shock-vortex-boundary layer interaction. Each of these three flowfields, combined with their respective comparisons to experiment or flight test, show the readiness of this method to impact the acquisition cycle of future fighters in the most demanding portions of the operational envelope.

References

[1] Spalart, P.R., "Strategies for turbulence modeling and simulation," 4th *International Symposium on Engineering Turbulence Modelling and Measurements*, Corsica, France, 1999.

[2] Strang, W.Z., Tomaro, R.F., Grismer, M.J., "The Defining Methods of Cobalt: A Parallel, Implicit, Unstructured Euler/Navier-Stokes Flow Solver," AIAA 99-0786, Jan., 1999.

[3] Forsythe, J.R., Hoffmann, K.A., Dieteker, F.F., "Detached-Eddy Simulation of a Supersonic Axisymmetric Base Flow with an Unstructured Flow Solver," AIAA 2000-2410, June, 2000.

[4] Morton, S.A., Forsythe, J.R., Mitchell, A.M., and Hajek, D., "DES and RANS Simulations of Delta Wing Vortical Flows," AIAA 2002-0587, January 2002.

[5] Forsythe, J., Squires, K., Wurtzler, K., and Spalart, P., "Detached Eddy Simulation of Fighter Aircraft at High Alpha," AIAA Paper 2002-0591, Jan., 2002.

[6] Morton, S., Steenman, M., Cummings, R., and Forsythe, J., "DES Grid Resolution Issues for Vortical Flows on a Delta Wing and an F/A-18*C*," AIAA 2003-1103, Jan., 2003.

[7] Forsythe, J.R., Woodson, S.H., "Unsteady CFD Calculations of Abrupt Wing Stall Using Detached-Eddy Simulation", AIAA 2003-0594, January, 2003.

[8] Samareh, J., "Gridtool: A Surface Modeling and Grid Generation Tool," *Proceedings of the Workshop on Surface Modeling, Grid Generation, and Related Issues in CFD Solution*, NASA CP-3291, May 9-11, 1995.

[9] Pirzadeh, S., "Progress Toward A User-Oriented Unstructured Viscous Grid Generator," AIAA Paper 96-0031, Jan., 1996.

[10] Spalart, P. R., and Allmaras, S.R., "A One Equation Turbulence Model for Aerodynamic Flows," *La Recherche Aerospatiale*, 1994, Vol. 1, p.5.

[11] Spalart, P. R. , Jou W-H. , Strelets M. , and Allmaras, S. R., "Comments on the Feasibility of LES for Wings, and on a Hybrid RANS/LES Approach," *Advances in DNS/LES, 1st AFOSR Int. Conf. on DNS/LES*, Aug 4-8, 1997, Greyden Press, Columbus Oh.

[12] Spalart, P., "Young-Person's Guide to Detached-Eddy Simulation Grids," NASA CR 2001-211032.

[13] Morton, S.A., Forsythe, J.R., Squires, K.D., and Wurtzler, K.E., "Assessment of Unstructured Grids for Detached-Eddy Simulation of High Reynolds Number Separated Flows," *8th ISGG Conference*, Honolulu, June, 2002.

[14] Pirzadeh, S., ``Vortical Flow Prediction Using an Adaptive Unstructured Grid Method", *Research & Technology Organization Applied Vehicle Technology Panel Meeting*, Norway, 7-11 May, 2001.

[15] Schuster, D., Byrd, J., "Transonic Unsteady Aerodynamics of the F/A-18E at Conditions Promoting Abrupt Wing Stall," AIAA Paper 2003-0593, January, 2003.